

SUPPLEMENTARY MATERIALS

Evaluation of thermal conductivity of organic phase-change materials from equilibrium and non-equilibrium molecular dynamics simulations: Paraffin as a test case

Victor M. Nazarychev,¹ Artyom D. Glova,¹ Igor V. Volgin,¹ Sergey V. Larin,¹ Alexey V. Lyulin,^{1,2} Sergey V. Lyulin,¹ Andrey A. Gurtovenko^{1,*}

¹ Institute of Macromolecular Compounds, Russian Academy of Sciences, Bolshoi Prospect V.O. 31, St. Petersburg, 199004, Russia. E-mail: a.gurtovenko@biosimu.org

² Theory of Polymers and Soft Matter Group, Technische Universiteit Eindhoven, P.O. Box 513, 5600 MB Eindhoven, The Netherlands

S1. GROMACS-to-LAMMPS conversion of atomistic force fields of n-eicosane

In our previous study [1] we explored the structural and dynamic properties of n-eicosane bulk samples with the use of the GROMACS package [2,3]. As the GROMACS suite lacks any in-built capabilities to compute the thermal conductivity, in this paper we employed the LAMMPS package [4] despite the fact that GROMACS is in general faster than LAMMPS, see Table S1 for a comparison of performance. Correspondingly, prior actual simulations, all 10 atomistic force fields of n-eicosane should be converted from GROMACS to LAMMPS. This was done with the use of the approach proposed in ref. [5].

In general, the total potential energy E_{pot} of a classical force field is given as:

$$E_{pot} = E_{bond} + E_{angle} + E_{dih} + E_{vdw} + E_{coul},$$

where E_{bond} , E_{angle} and E_{dih} are the energies of bond, angle and dihedral interactions, E_{vdw} is the energy of the van der Waals interactions, and E_{coul} is the energy of the Coulomb interactions. Each atomistic force field of n-eicosane has its own unique set of potential functions and parameters of these functions to describe the interactions in a system [1]. After the GROMACS-to-LAMMPS conversion was performed, the correctness of the conversion was validated via a direct comparison of various energy components extracted from GROMACS and LAMMPS simulations [6,7]. To this end, a short 100 ps NVT simulations were performed with the use of both packages.

Overall, we were able to make a straightforward GROMACS-to-LAMMPS conversion for most force fields with two exceptions: CHARMM36 and GROMOS force fields. In both these force fields 1-4 interactions are accounted for through the scaling and with the use of a separate set of Lennard-Jones (van der Waals) parameters [8–11]. As the separate sets of 1-4 interactions are not supported in the LAMMPS package, a proper implementation of CHARMM36 and GROMOS force fields required special consideration. In particular, for the CHARMM36 force field we used a previously established approach: the 1-4 Lennard-Jones interactions were turned off and the dihedral interactions were simultaneously corrected [12]. In turn, for the GROMOS

force field we found that scaling the 1-4 Lennard-Jones interactions by a factor of 0.05 gives the best agreement between the energies produced by both simulation packages at T=250 K (the crystalline phase). However, for the liquid state (T=450 K) this approach did not work. Instead, we found that the best match is achieved when the 1-4 Lennard-Jones interactions are completely switched off.

In Fig. S1–S5 we compare the component-wise energies measured in both simulation packages for all 10 force fields, in liquid and crystalline phases. To this end, we focused on the ratio of the potential energies ($E_{\text{LAMMPS}}/E_{\text{GROMACS}}$); the best agreement between LAMMPS and GROMACS packages is achieved when the $E_{\text{LAMMPS}}/E_{\text{GROMACS}}$ approaches 1. It is seen that for most force fields only minor (less than 5%) deviations in the energy components are observed during simulations performed by LAMMPS and GROMACS packages. The only exceptions are CHARMM36 and GROMOS force fields for which the energy components measured in LAMMPS and GROMACS simulations differ to a somewhat greater extent (less than 10%), see Fig. S5.

Table S1. Computational performance of 10 atomistic force fields of n-eicosane samples at T = 450K in molecular dynamics simulations performed with the GROMACS (version 5.1.4) and LAMMPS (version 15 Apr 2020) packages. The GROMACS simulations were carried out on 70 CPU cores (Intel Xeon CPU E5-2697 v3) of the Lomonosov-2 supercomputer. The LAMMPS simulations were performed on 64 CPU cores (Intel Xeon E5450) of the Kurchatov Institute supercomputer.

Force field	Performance, ns/day	
	GROMACS	LAMMPS
CHARMM36	52.4	1.3
GAFF	83.6	1.1
GAFF2	85.7	1.1
L-OPLS-AA	47.4	0.5
OPLS-AA	46.9	0.5
NERD	556.3	3.9
OPLS-UA	395.9	2.5
PYS	693.4	5.3
TraPPE	443.1	3.2
GROMOS	463.6	3.8

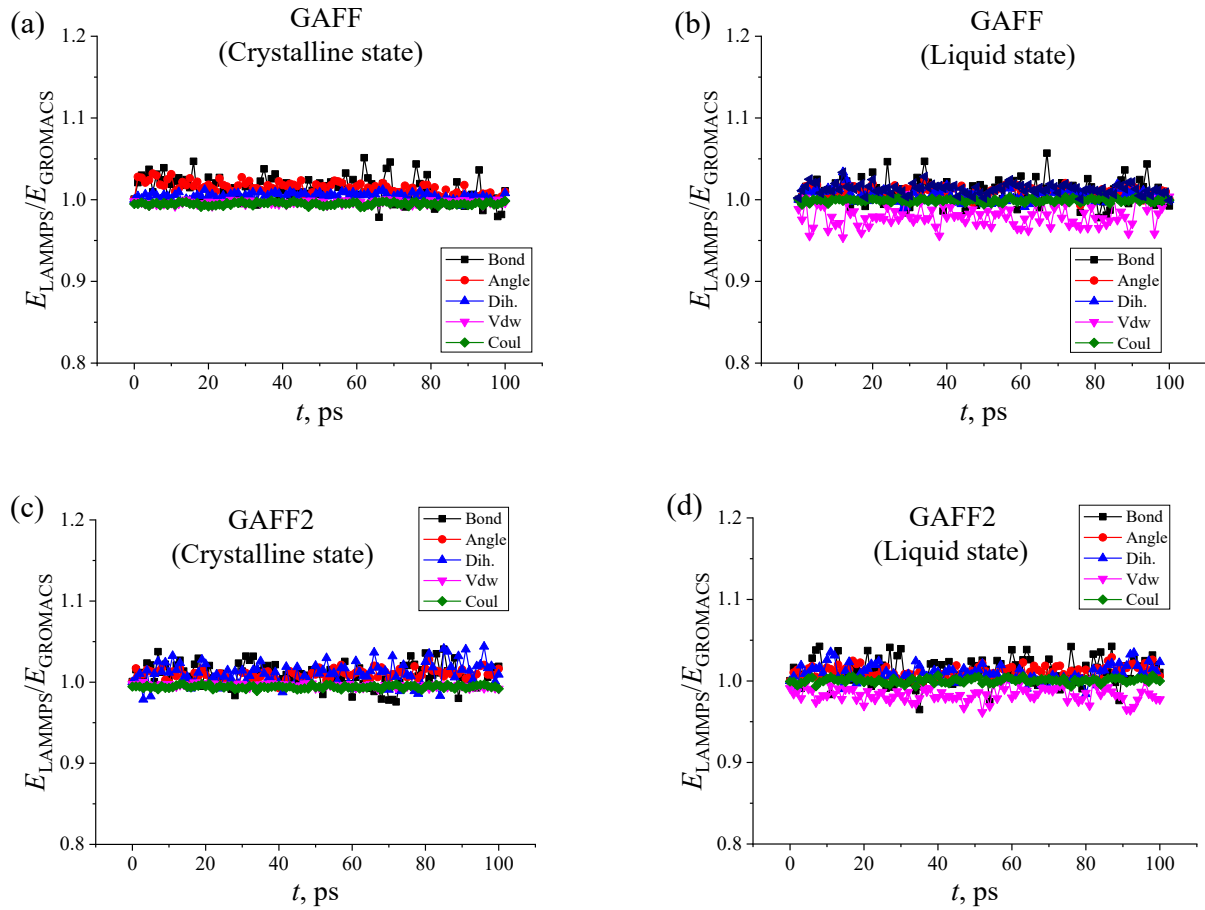


Figure S1. The ratio $E_{\text{LAMMPS}}/E_{\text{GROMACS}}$ for various energy components as a function of time. Shown are the results for the GAFF and GAFF2 force fields in the crystalline ($T=250$ K) and in the liquid ($T=450$ K) states. The energy components that correspond to the bond (Bond), the valent angle (Angle), the dihedrals (Dih.), the van der Waals (Vdw), and the Coulomb (Coul) interactions are presented.

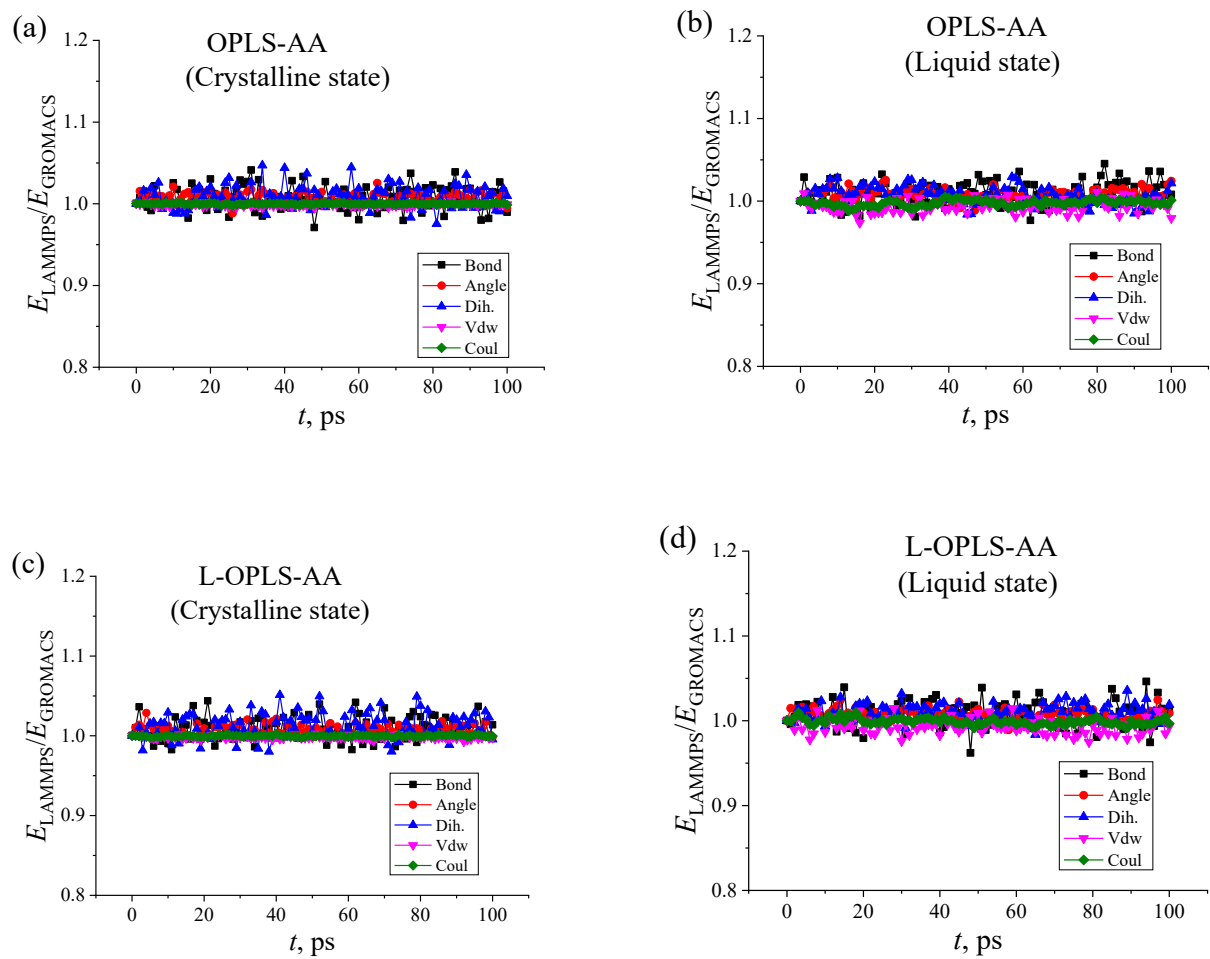


Figure S2. The ratio $E_{\text{LAMMPS}}/E_{\text{GROMACS}}$ for various energy components as a function of time. Shown are the results for the OPLS-AA and L-OPLS-AA force fields in the crystalline ($T=250$ K) and in the liquid ($T=450$ K) states.

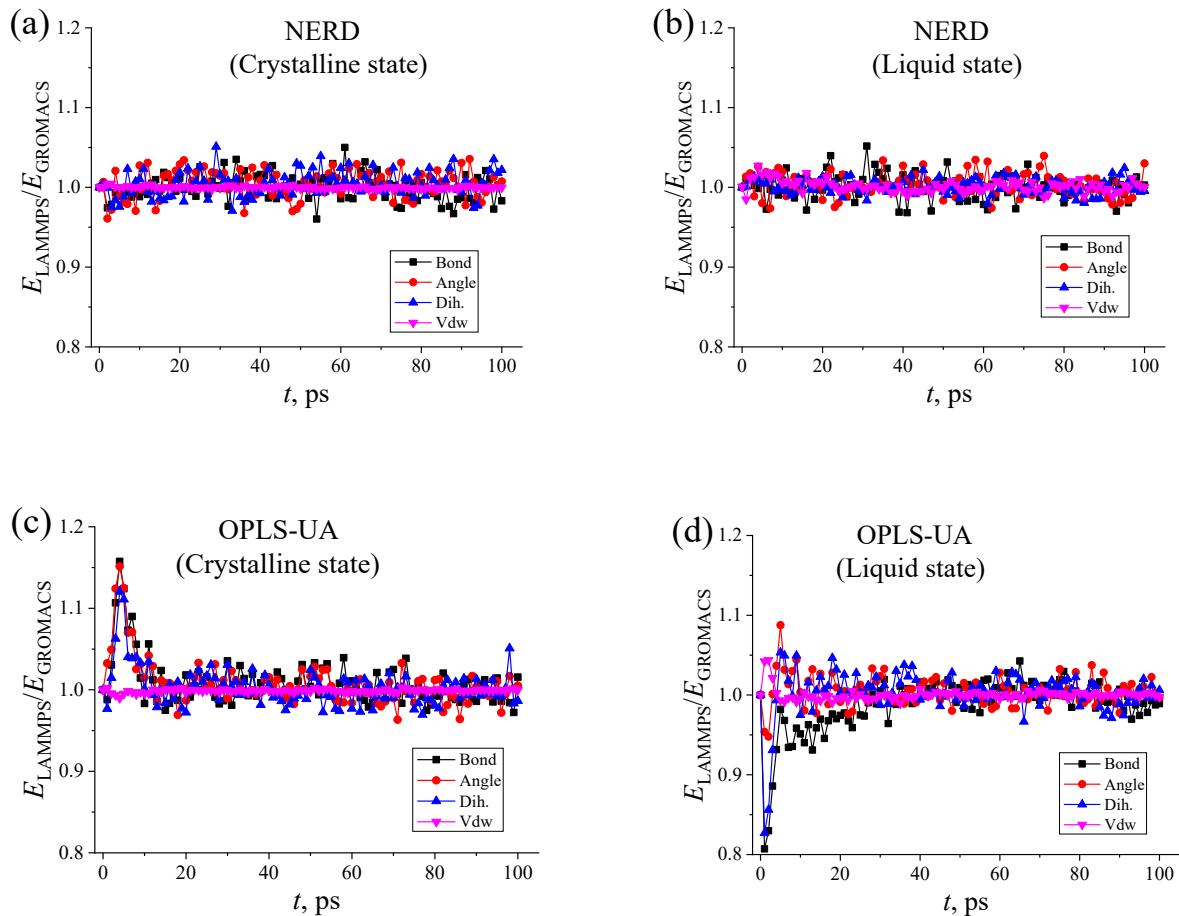


Figure S3. The ratio $E_{\text{LAMMPS}}/E_{\text{GROMACS}}$ for various energy components as a function of time. Shown are the results for the NERD and OPLS-UA force fields in the crystalline (T=250 K) and in the liquid (T=450K) states.

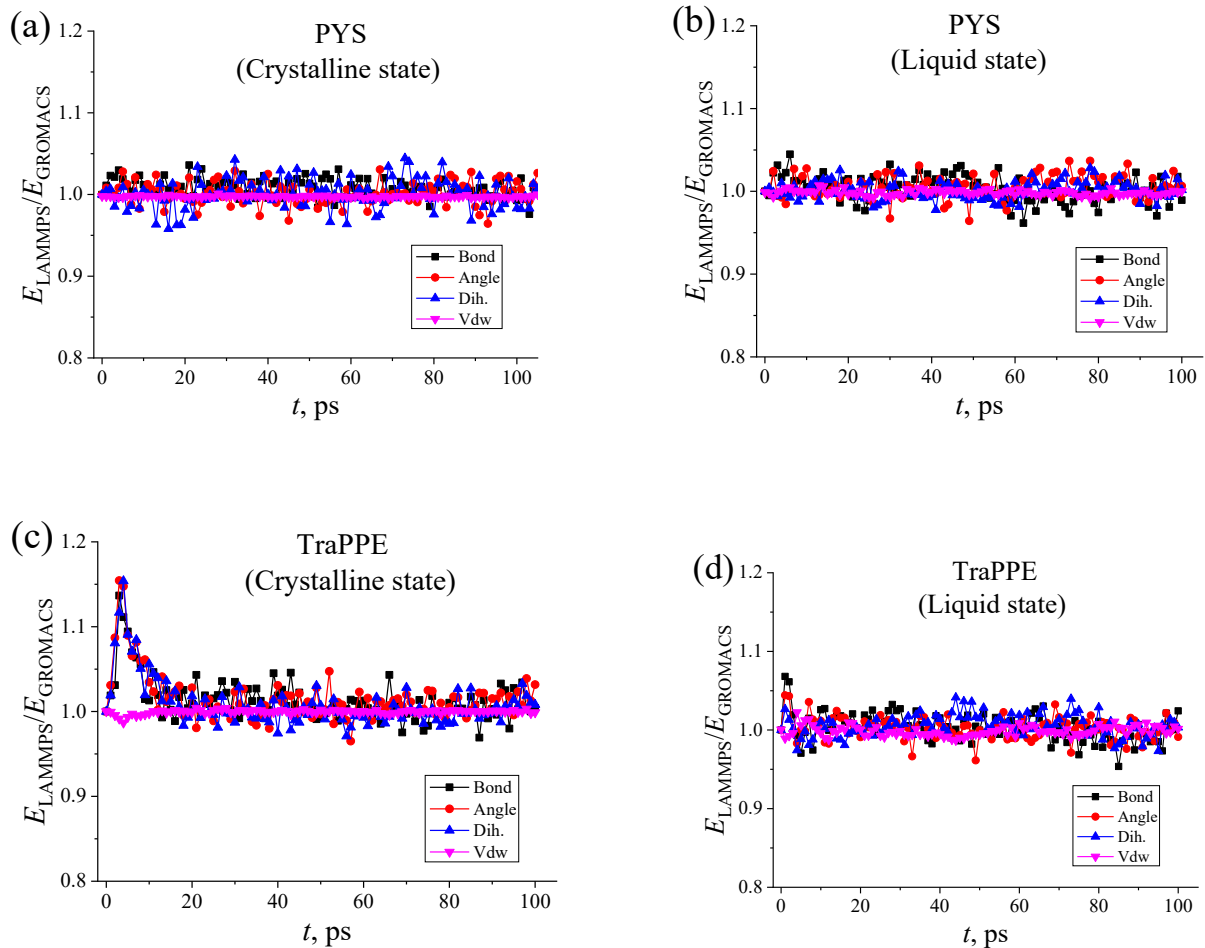


Figure S4. The ratio $E_{\text{LAMMPS}}/E_{\text{GROMACS}}$ for various energy components as a function of time. Shown are the results for the PYS and TraPPE force fields in the crystalline ($T=250$ K) and in the liquid ($T=450$ K) states.

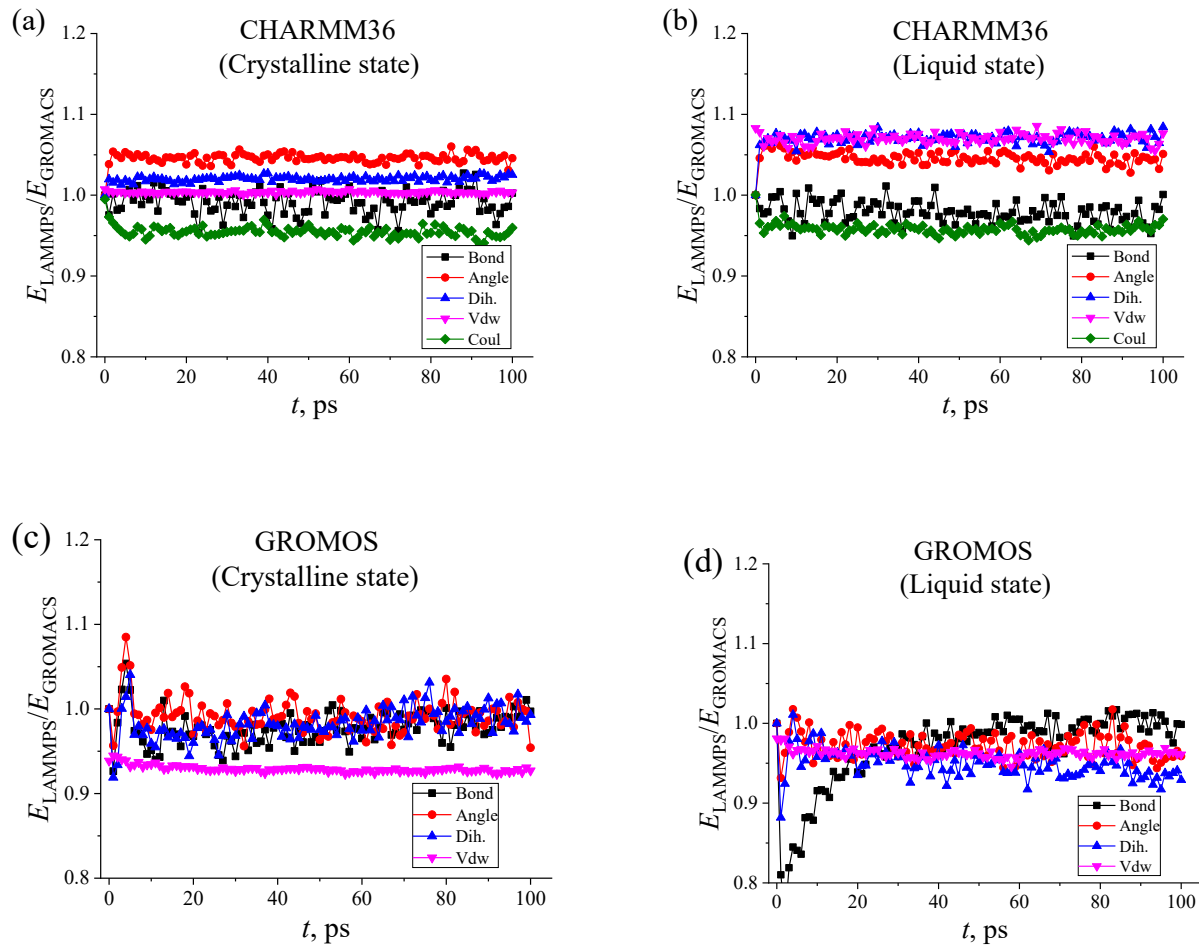


Figure S5. The ratio $E_{\text{LAMMPS}}/E_{\text{GROMACS}}$ for various energy components as a function of time. Shown are results for the CHARMM36 and GROMOS force fields in the crystalline ($T=250$ K) and in the liquid ($T=450$ K) states.

S2. Autocorrelation functions of heat flux and thermal conductivity coefficient

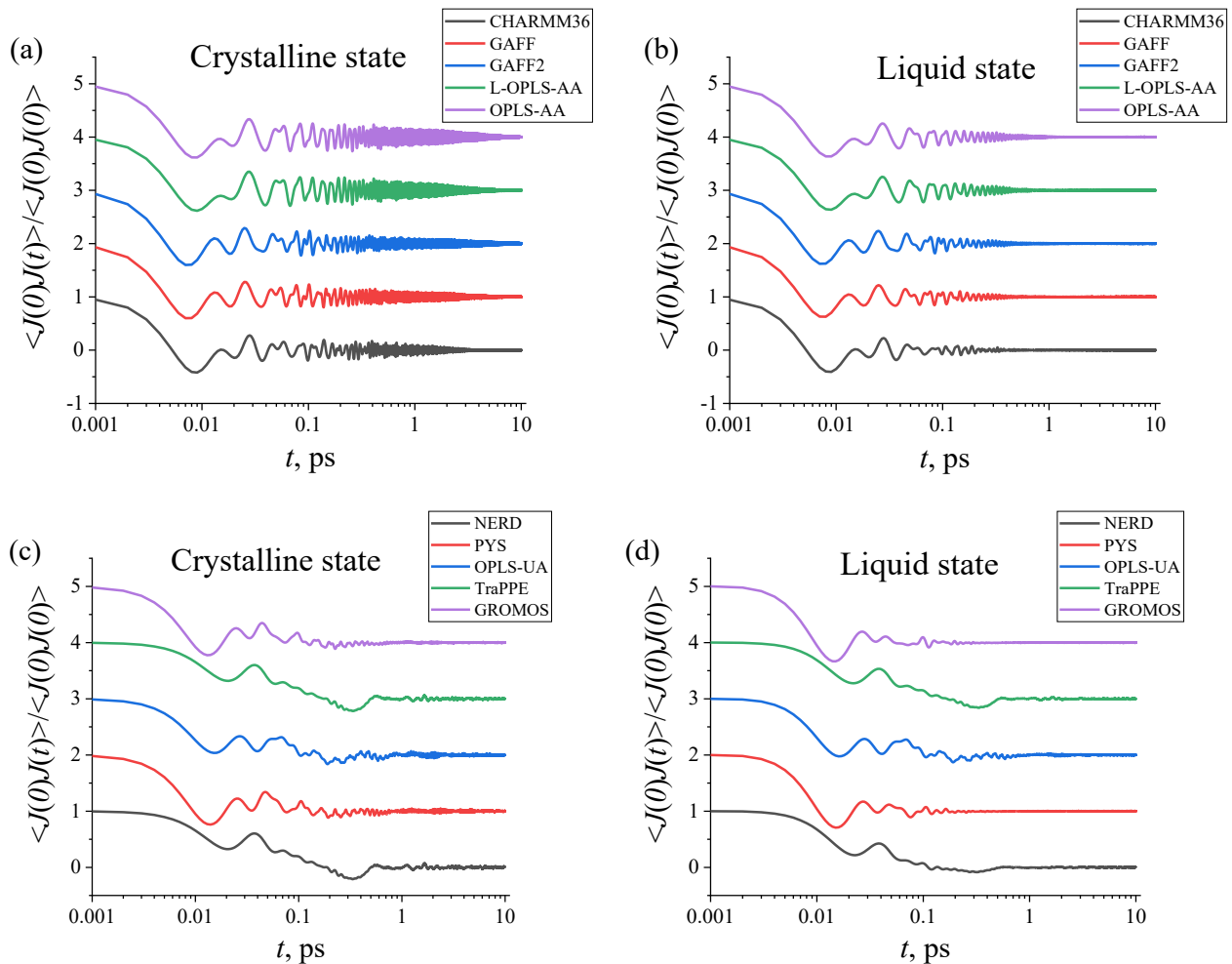


Figure S6. Autocorrelation functions of the heat flux (HFACF) for n-eicosane in the crystalline and in the liquid states as a function of time. For clarity's sake, the curves for the different force fields are arbitrary shifted from each other.

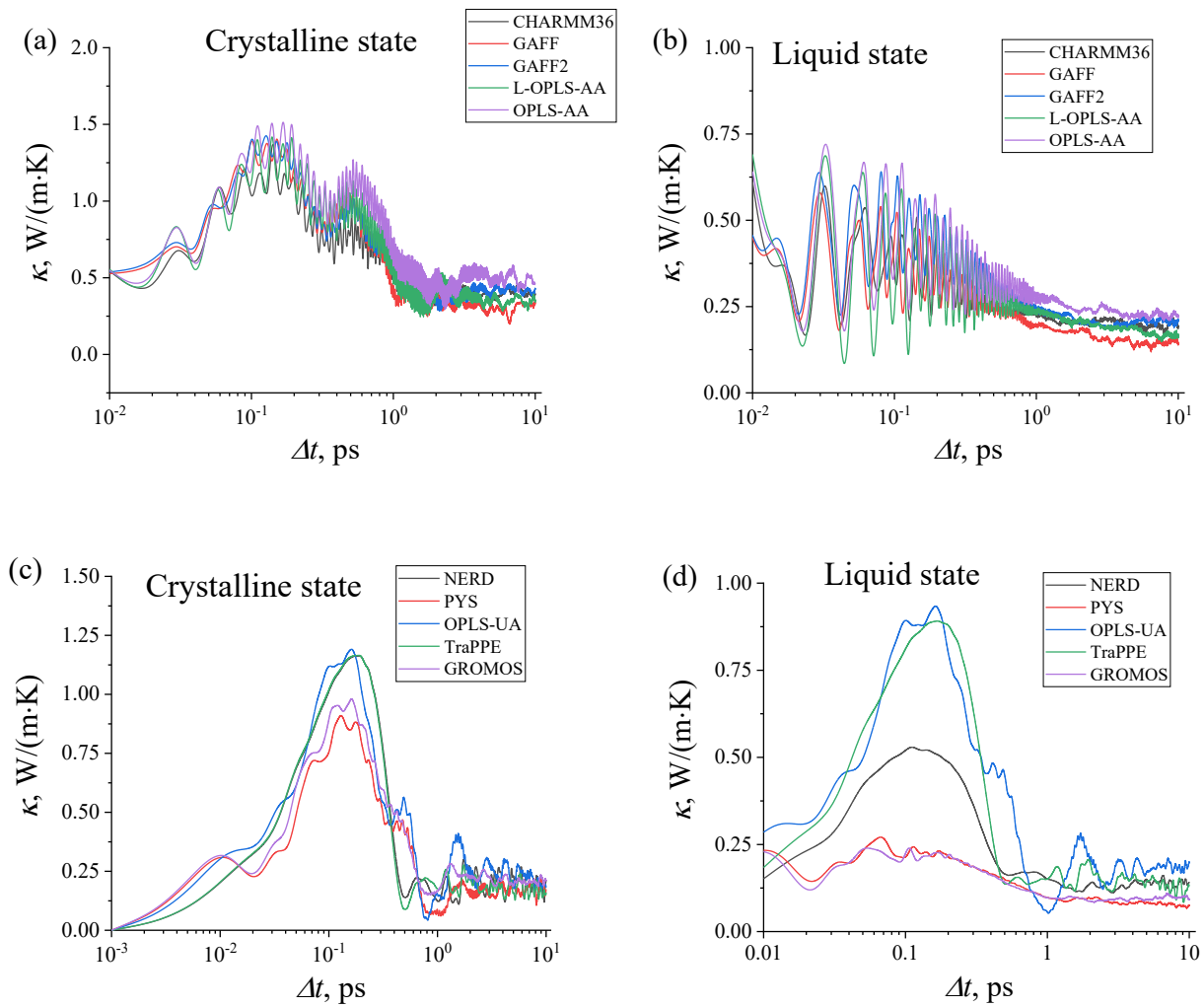


Figure S7. The thermal conductivity coefficient as a function of a time interval Δt used for the integration of HFACF in eq. (2). The last 10 ps of 1 ns EMD trajectories were used for the analysis. Shown are the results for 10 force fields of n-eicosane, for the crystalline ($T=250$ K) and for the liquid ($T=450$ K) phases.

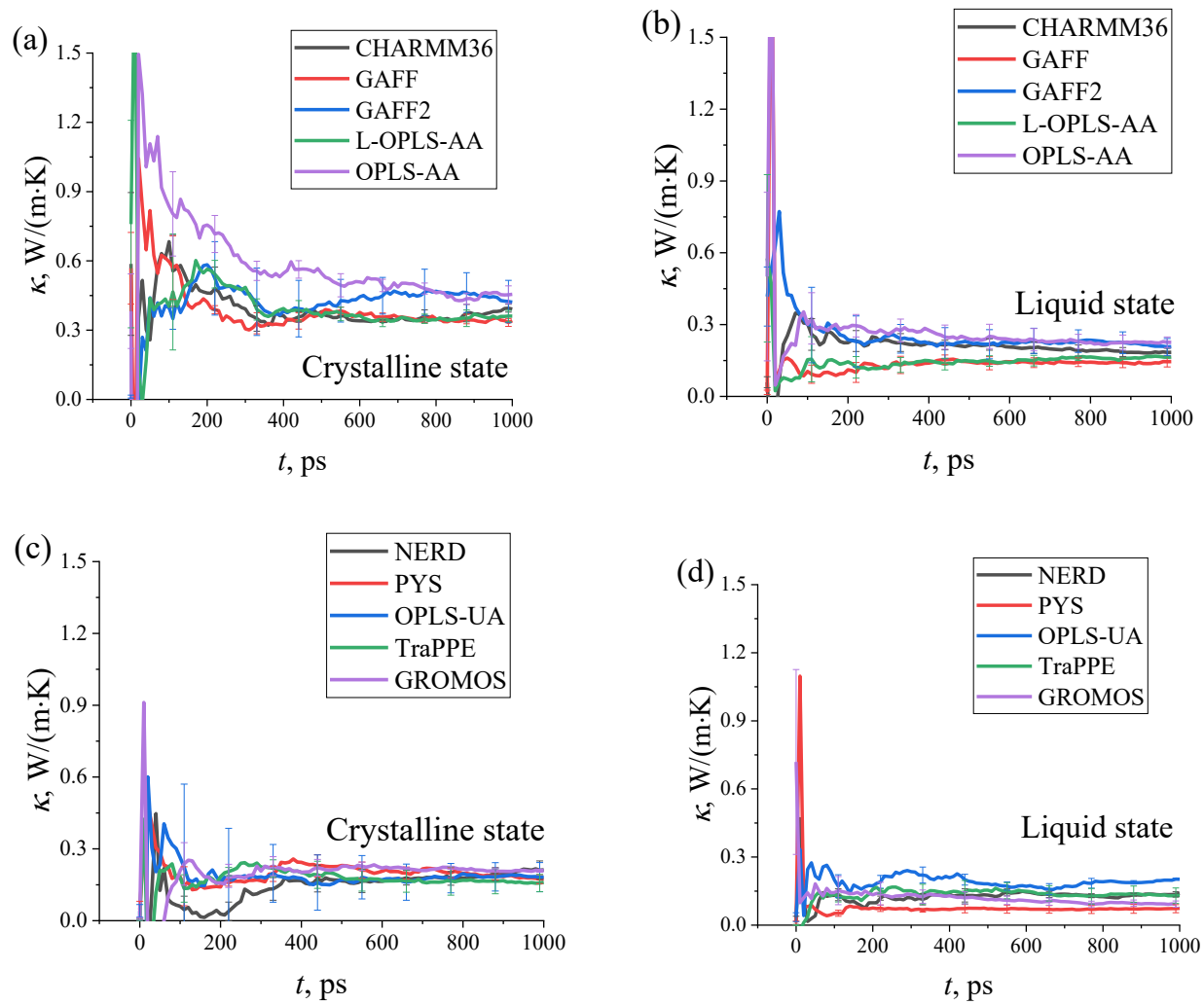


Figure S8. The thermal conductivity coefficient κ calculated over 1 ns trajectory with a time step of 10 ps for each force field and for both crystalline and liquid states.

S3. Autocorrelation functions of the C-C bond vector

To evaluate the stiffness of the paraffin chain in different force fields, we analyzed the local orientational mobility of the C-C bond vector. Since the stiffness itself should not depend on the phase, we chose to study the local orientational relaxation of paraffin in the liquid phase ($T = 450$ K). To this end, we calculated the autocorrelation function $P_I(t)$ of the C-C bond vector:

$$P_I(t) = \langle \vec{b}(t_0) \cdot \vec{b}(t + t_0) \rangle, \quad (\text{S1})$$

where b is the unit vector along the C-C bond at time t_0 and time $t + t_0$; the brackets $\langle \dots \rangle$ indicate the averaging over time and over all vectors in a simulation box. The autocorrelation functions $P_I(t)$ calculated for 10 force fields are shown in Fig. S9.

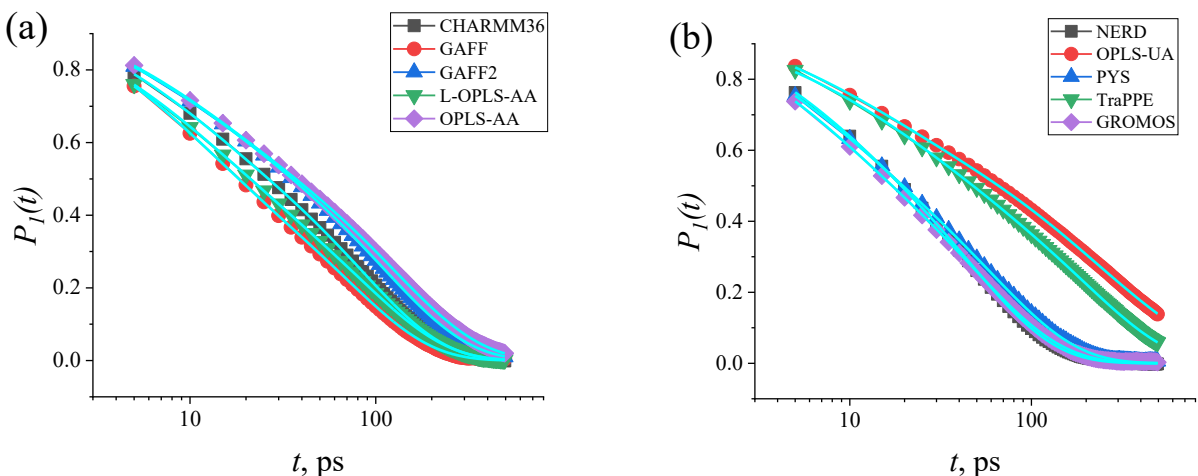


Figure S9. Time dependence of the autocorrelation function $P_I(t)$ for the C-C bond vector for all-atom (a) and united-atom (b) models for paraffin samples in the liquid phase at $T=450$ K. Each $P_I(t)$ was calculated by averaging over 3 n-eicosane samples. The fitting of $P_I(t)$ with the Kohlrausch-Williams-Watts function is shown by cyan lines.

To evaluate the characteristic relaxation times of the autocorrelation functions $P_I(t)$ for different computational models, the time dependence of $P_I(t)$ was approximated by the sum of two Kohlrausch-Williams-Watts stretched exponents:

$$f(t) = A e^{-(t/\tau_1)^{\beta_1}} + (1-A) e^{-(t/\tau_2)^{\beta_2}}, \quad (\text{S2})$$

where $A \leq 1$, τ_1 and τ_2 are the characteristic relaxation times, and β_1 and β_2 are parameters accounting for the non-exponentiality of the relaxation process. Instead of τ_1 and τ_2 , one can consider a cumulative relaxation time (the mean correlation time), τ_c defined as

$$\tau_c = \int_0^\infty P_1(t) dt = A \frac{\tau_1}{\beta_1} \Gamma\left(\frac{1}{\beta_1}\right) + (1-A) \frac{\tau_2}{\beta_2} \Gamma\left(\frac{1}{\beta_2}\right), \quad (\text{S3})$$

where Γ is the Gamma function. The outcome of the approximation of the autocorrelation functions $P_1(t)$ is summarized in Table S2.

Table S2. The parameters of the two Kohlrausch-Williams-Watts functions used to approximate the autocorrelation functions $P_1(t)$ for different force fields at $T=450$ K, see Fig. S9.

Force Field	A	τ_1 , ps	τ_2 , ps	β_1	β_2	τ_c , ps
CHARMM36	0.65 ± 0.02	87 ± 3	7.8 ± 0.5	1.00 ± 0.03	0.84 ± 0.04	60
GAFF	0.57 ± 0.03	75 ± 3	8.1 ± 0.4	1.00 ± 0.03	0.88 ± 0.03	46
GAFF2	0.68 ± 0.01	112 ± 1	8.3 ± 0.2	0.95 ± 0.01	0.78 ± 0.02	81
L-OPLS-AA	0.57 ± 0.01	89 ± 1	8.6 ± 0.1	0.99 ± 0.01	0.79 ± 0.01	55
OPLS-AA	0.67 ± 0.01	128 ± 1	8.9 ± 0.1	0.94 ± 0.01	0.80 ± 0.01	91
NERD	0.76 ± 0.02	47 ± 1	5.4 ± 0.3	0.95 ± 0.02	0.89 ± 0.04	38
OPLS-UA	0.76 ± 0.01	234 ± 3	9.2 ± 0.2	0.70 ± 0.01	0.75 ± 0.02	227
PYS	0.66 ± 0.03	63 ± 3	6.5 ± 0.5	0.95 ± 0.03	0.84 ± 0.05	45
TraPPE	0.55 ± 0.02	223 ± 6	16.7 ± 0.9	1.00 ± 0.02	0.66 ± 0.01	131
GROMOS	0.71 ± 0.03	50 ± 2	5.3 ± 0.4	0.91 ± 0.03	0.90 ± 0.07	38

Analysis of Table S2 and Fig. S10 shows that for both all-atom and united-atom force fields there is a correlation between the relaxation time τ_c of the C-C bond vector and the thermal conductivity coefficient of a paraffin sample in the crystalline state. More specifically, the slower local orientational mobility (the longer relaxation time τ_c), the larger thermal conductivity coefficient κ .

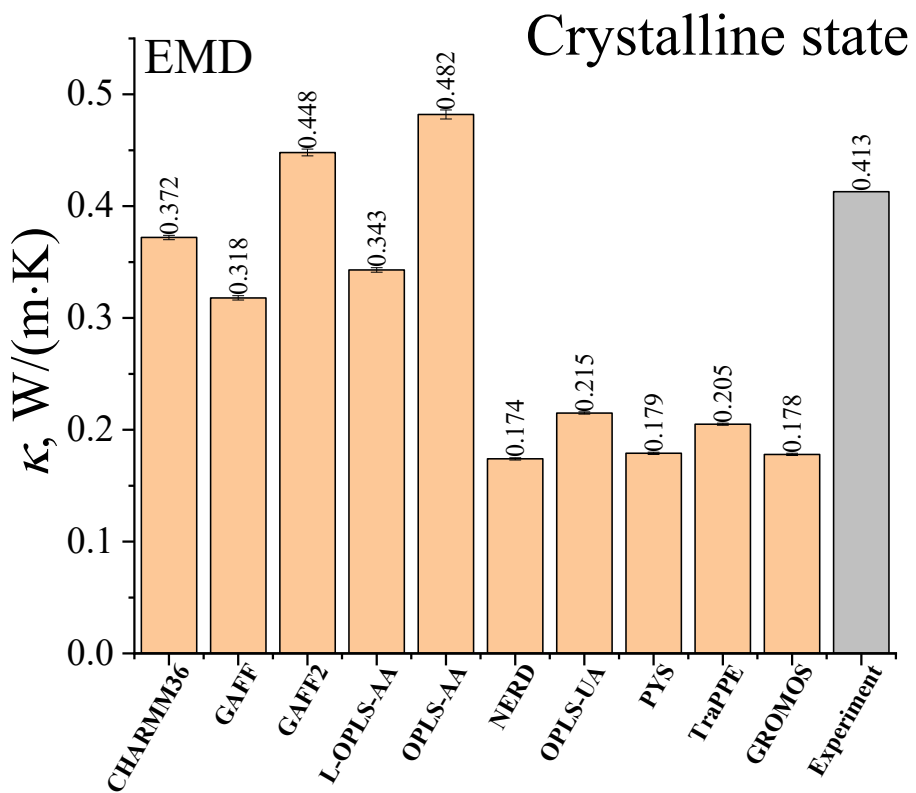


Figure S10. The coefficient of thermal conductivity κ of n-eicosane samples in the crystalline state ($T = 250$ K) for different force fields (EMD simulations).

S4. Temperature gradient

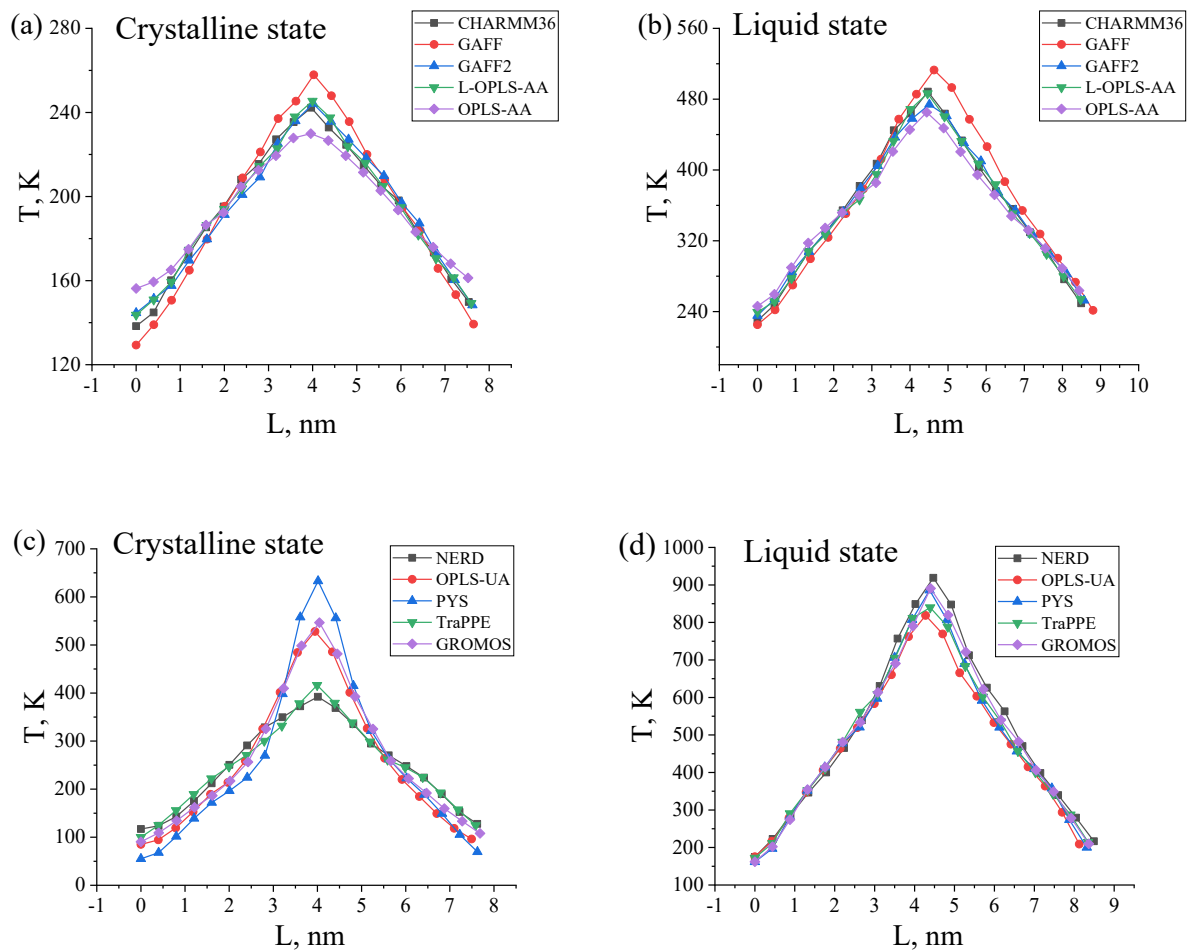


Figure S11. The temperature profiles as function of the position in a simulation box along the direction of the heat flux. Shown are the results for 10 force fields and for both crystalline ($T=250\text{ K}$) and liquid ($T=450\text{ K}$) phases.

S5. Equilibrium versus non-equilibrium methods

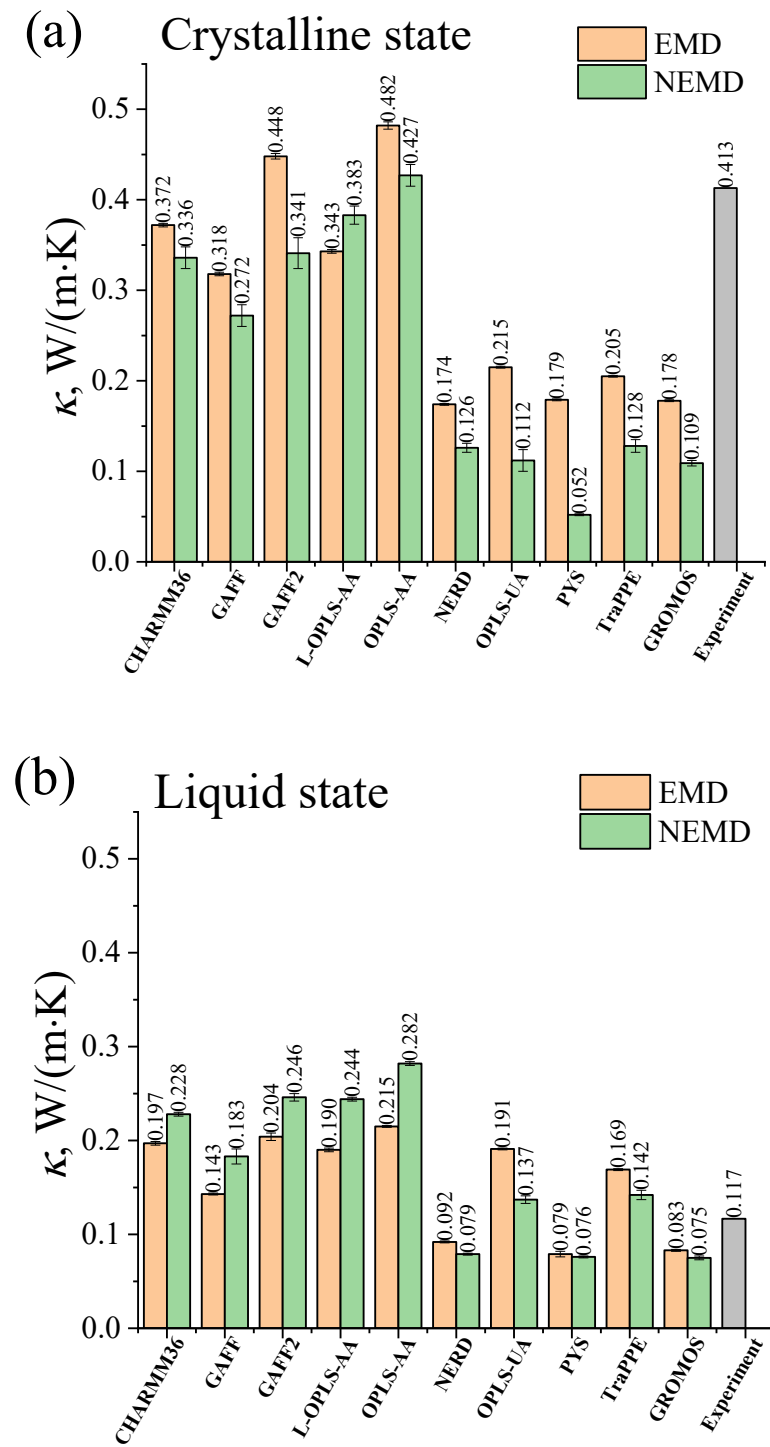


Figure S12. The thermal conductivity coefficients of n-eicosane in the crystalline (a) and in the liquid (b) states of the n-eicosane samples. Shown are the results for EMD and NEMD simulations, as well as the experimental data [13,14].

References

1. Glova, A. D.; Volgin, I. V; Nazarychev, V. M.; Larin, S. V.; Lyulin, S. V.; Gurtovenko, A. A. Toward realistic computer modeling of paraffin-based composite materials: critical assessment of atomic-scale models of paraffins. *RSC Advances* **2019**, *9*, 38834–38847, doi:10.1039/C9RA07325F.
2. van der Spoel, D.; Lindahl, E.; Hess, B.; Groenhof, G.; Mark, A. E.; Berendsen, H. J. C. GROMACS: fast, flexible, and free. *Journal of Computational Chemistry* **2005**, *26*, 1701–18, doi:10.1002/jcc.20291.
3. Hess, B.; Kutzner, C.; van der Spoel, D.; Lindahl, E. GROMACS 4: Algorithms for highly efficient, load-balanced, and scalable molecular simulation. *Journal of Chemical Theory and Computation* **2008**, *4*, 435–447, doi:10.1021/ct700301q.
4. Plimpton, S. Fast parallel algorithms for short-range molecular dynamics. *Journal of Computational Physics* **1995**, *117*, 1–19, doi:10.1006/jcph.1995.1039.
5. Shirts, M. R.; Klein, C.; Swails, J. M.; Yin, J.; Gilson, M. K.; Mobley, D. L.; Case, D. A.; Zhong, E. D. Lessons learned from comparing molecular dynamics engines on the SAMPL5 dataset. *Journal of Computer-Aided Molecular Design* **2017**, *31*, 147–161, doi:10.1007/s10822-016-9977-1.
6. Rusu, V. H.; Horta, V. A. C.; Horta, B. A. C.; Lins, R. D.; Baron, R. MDWiZ: A platform for the automated translation of molecular dynamics simulations. *Journal of Molecular Graphics and Modelling* **2014**, *48*, 80–86, doi:10.1016/j.jmgm.2013.12.006.
7. Chávez Thielemann, H.; Cardellini, A.; Fasano, M.; Bergamasco, L.; Alberghini, M.; Ciorra, G.; Chiavazzo, E.; Asinari, P. From GROMACS to LAMMPS: GRO2LAM. *Journal of Molecular Modeling* **2019**, *25*, 147, doi:10.1007/s00894-019-4011-x.
8. Klauda, J. B.; Venable, R. M.; Freites, J. A.; O'Connor, J. W.; Tobias, D. J.;

- Mondragon-Ramirez, C.; Vorobyov, I.; MacKerell, A. D.; Pastor, R. W. Update of the CHARMM all-atom additive force field for lipids: validation on six lipid types. *Journal of Physical Chemistry B* **2010**, *114*, 7830–7843, doi:10.1021/jp101759q.
9. Klauda, J. B.; Brooks, B. R.; MacKerell, A. D.; Venable, R. M.; Pastor, R. W. An ab initio study on the torsional surface of alkanes and its effect on molecular simulations of alkanes and a DPPC bilayer. *Journal of Physical Chemistry B* **2005**, *109*, 5300–11, doi:10.1021/jp0468096.
10. Schuler, L. D.; Daura, X.; Van Gunsteren, W. F. An improved GROMOS96 force field for aliphatic hydrocarbons in the condensed phase. *Journal of Computational Chemistry* **2001**, *22*, 1205–1218, doi:10.1002/jcc.1078.
11. Oostenbrink, C.; Villa, A.; Mark, A. E.; van Gunsteren, W. F. A biomolecular force field based on the free enthalpy of hydration and solvation: The GROMOS force-field parameter sets 53A5 and 53A6. *Journal of Computational Chemistry* **2004**, *25*, 1656–1676, doi:10.1002/jcc.20090.
12. LAMMPS Online Documentation,
https://lammps.sandia.gov/doc/special_bonds.html (accessed on Jul 14, 2020).
13. Griggs, E. I.; Yarbrough, D. W. Thermal conductivity of solid unbranched alkanes from n-hexadecane to n-eicosane. In Proceedings of the Southeastern Seminar on Thermal Sciences; North Carolina State University, 1978; pp. 256–257.
14. Rastorguev, Y. L.; Bogatov, G. F.; Grigor'ev, B. A. Thermal conductivity of higher n-alkanes. *Chemistry and Technology of Fuels and Oils* **1974**, *10*, 728–732, doi:10.1007/BF00717208.